The Single-crystal Electron Spin Resonance Spectrum of *N,N,N',N'*-Tetramethylethylenediaminedium Aquabis(malonato)oxovanadate(IV) Dihydrate, A Weak Two-dimensional Exchanging System †

David Collison, Brendan Gahan, and Frank E. Mabbs *
Chemistry Department, University of Manchester, Manchester M13 9PL

Single-crystal e.s.r. spectra of the title compound $[H_2tmen][VO(mal)_2(H_2O)]\cdot 2H_2O$ over the temperature range 310—4.2 K are reported. The crystal structure shows the presence of two-dimensional layers of anions in the crystal, with all V=O vectors perpendicular to these layers. The e.s.r. spectra with the applied magnetic field parallel to the V=O direction are compatible with a weak isotropic exchange interaction, J_0, within this layer, and have been simulated on this basis. It is shown that J_0 varies almost linearly in magnitude, and changes sign, with temperature, being *ca.* −200 G (ferromagnetic) at 300 K, changing sign at *ca.* 190 K, and *ca.* +290 G (antiferromagnetic) at 4.2 K. Possible mechanisms for the isotropic exchange, and reasons for its variation with temperature, are discussed.

The effects on the e.s.r. spectrum of an undiluted transition-metal complex due to (*i*) nuclear hyperfine interactions,[1] (*ii*) the formation of discrete polymeric units,[1-3] (*iii*) strong electronic exchange over a large number of paramagnetic centres,[1,4-7] (*iv*) the interaction with adjacent magnetic dipoles,[1] and (*v*) weak electronic exchange over many centres wherein the exchange between adjacent centres is comparable to or less than the metal hyperfine interaction[8-10] were discussed in the introduction to the preceding paper.[10]

The situation represented by (*v*) seems to be relatively rare, and has only been reported for *cis*-$[VO(pbd)_2]$,[8] $[NBu^n_4]_2[Cu(mnt)_2]$,[9] and $[VOX_2(tmu)_2]$.[10,‡] Weak inter-dimer exchange in bis[3,9-bis(dimethylamino)phenazothionium] bis(maleonitriledithiolato)cuprate(II)–acetone has also been reported to give rise to additional weak e.s.r. resonances.[11] A consideration of these examples suggested that the extended weak exchange in (*v*) probably requires particular structural conditions. These constraints probably demand a lack of clustering within a reference unit cell, the close approach of paramagnetic centres to within about 6—10 Å, and a repeating pattern of molecules or ions throughout one, two, or three dimensions in the crystal. The crystal structure of the compound $[H_2tmen][VO(mal)_2(H_2O)]\cdot 2H_2O$, where H_2tmen = *N,N,N',N'*-tetramethylethylenediaminedium and mal = malonate, suggested the presence of a two-dimensional layer of the anions.[12] Thus we now report the single-crystal e.s.r. spectra of this compound at *X*-band frequencies over the temperature range 4.2—310 K. The spectra are analysed using the theoretical model developed in the preceding paper.[10]

Experimental

The salt $[H_2tmen][VO(mal)_2(H_2O)]\cdot 2H_2O$ was prepared according to the method of Pajunen and Pajunen.[12] Single crystals were grown directly from the preparative solutions.

E.s.r. spectra were obtained on oriented (by standard *X*-ray techniques) single crystals over the temperature range 300—4.2 K at *X*-band frequencies using a Varian E112 spectrometer, by methods previously described.[13] The crystals were cooled using an Oxford Instruments ESR 9 continuous flow cryostat fitted with a goniometer so that the cooled crystals could be rotated through 360° in a horizontal plane. Temperature measurement and control was achieved *via* a 0.3% Fe–Au thermocouple and a Harwell DT temperature controller. The temperature was controlled to better than ±0.5 K over the whole range. The crystals were mounted such that spectra could be obtained in the crystallographic *ac*, *bc*, and *ab* planes.

Results and Discussion

The variations of the *X*-band e.s.r. spectra with temperature in the range 310—4.2 K and with the applied magnetic field parallel to the crystallographic *c* axis (molecular *z* axis, $\theta = 0°$, see below) are shown in Figure 1. The changes in the spectra were completely reversible with respect to changing temperature over the entire range of temperature. The total spectrum width (between the points marked * on each spectrum) varied markedly with temperature. It decreased from 2 400 G at 310 K to a minimum of 1 425 G at 190 K, from which it then increased with decreasing temperature to 2 440 G at both 30 and 4.2 K. The form of the spectra at most temperatures within the range followed a similar pattern, *i.e.* a clearly resolved weak feature (*) at each extremity, with (generally) more intense features which varied in number and relative intensity between the extremities. The exceptions to this pattern occurred in the range 210—160 K where the extreme features were the most intense, and only eight features were resolved. To a first approximation the second half of each spectrum is the inverse of the first half. The angular variation of the e.s.r. spectrum in the crystallographic *bc* plane at a number of selected temperatures is shown in Figures 2—6. In these figures θ is the angle between the applied magnetic field and the crystallographic *c* axis. A number of qualitatively similar changes are observed in the angular variations of the spectra at each temperature. The total width of the spectra is greatest for $\theta = 0°$ and narrowest for $\theta = 90°$. A decrease in resolution within the spectra also accompanies this decrease in total width. Although we only report the *X*-band spectra in detail, we have found that *Q*-band spectra are identical at the same temperatures.

A prerequisite for the interpretation of the e.s.r. spectra of $[H_2tmen][VO(mal)_2(H_2O)]\cdot 2H_2O$ is a description of its crystal structure. The compound crystallises in the orthorhombic space group *Pnma*, with four formula units in the unit cell.[12] The vanadium atom is approximately octahedrally co-ordinated to four malonato-oxygens and to the terminal 'vanadyl' oxygen *trans* to which is an oxygen atom of one water molecule, see Figures 7 and 8. The vanadium–terminal

† *Non-S.I. unit employed:* $G = 10^{-4}$ T.
‡ See ref. 10 for ligand abbreviations.

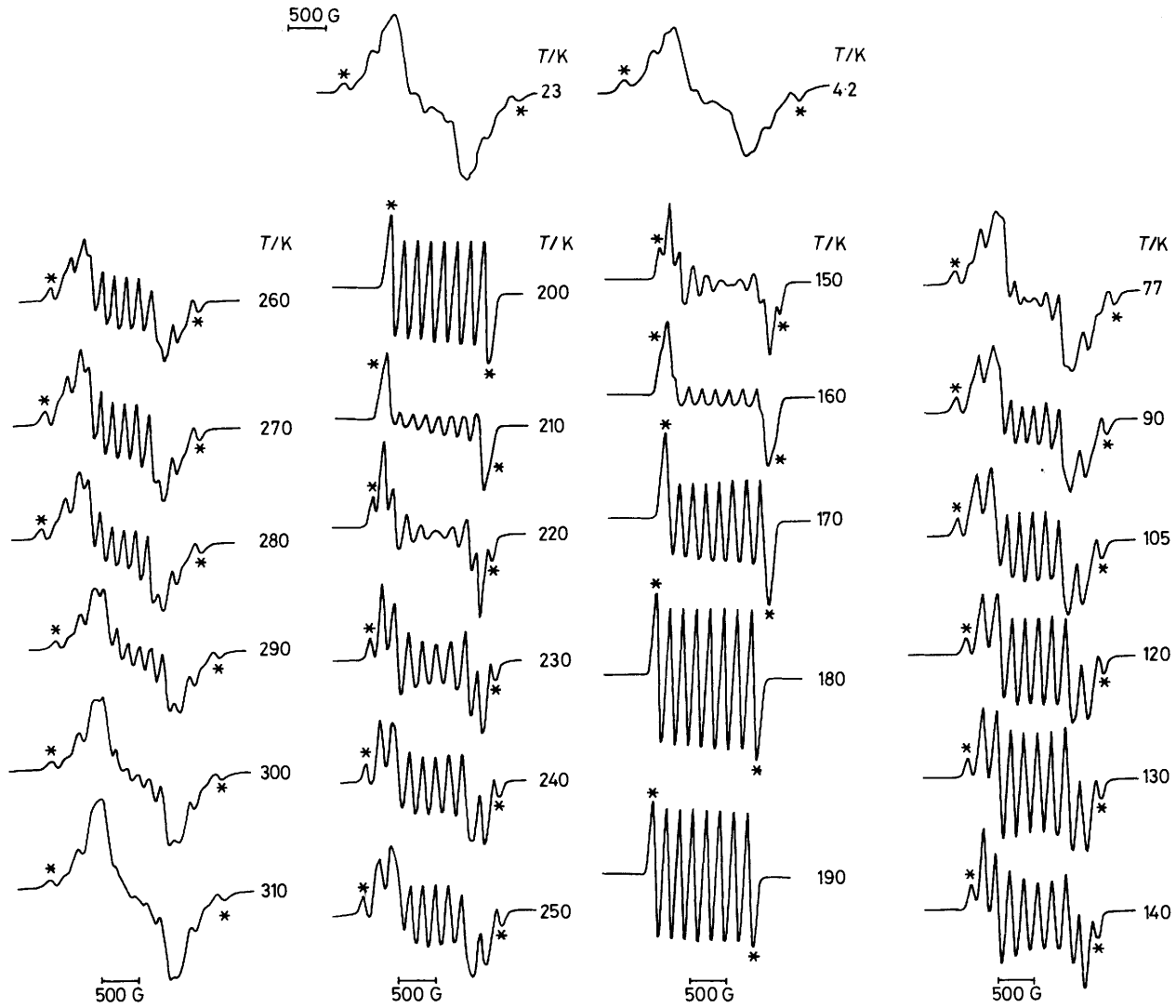

Figure 1. Variation of the e.s.r. spectrum with temperature when the applied magnetic field is parallel to the *c* axis

oxygen vectors of each anion lie within 0.5° of the crystallographic *c* axis. In view of this small angle we have assumed the molecular *z* axis to be parallel to *c*. This is probably a reasonable assumption since subsequent simulations of the e.s.r. spectra show no detectable changes for a one degree change in the applied magnetic field with respect to the *c* axis. E.s.r. spectra recorded in the crystallographic *ab* plane were compatible with axial symmetry for the *g* and *A* tensors. Thus all molecules in the unit cell are effectively magnetically equivalent at any orientation of the applied magnetic field. Hydrogen bonding between the anions and water molecules results in the formation of a layer parallel to the *ac* plane,[12] in which there is considerable ordering, see Figure 8. Within this layer there are three relatively close vanadium–vanadium distances, r_1 (6.342), r_2 (8.531), and r_3 (9.434 Å). The layers parallel to the *ac* plane are separated from each other by 9.256 Å due to the intervention of the cations, see Figure 7.

Structural considerations, plus a comparison of the form of many of the spectra with those observed for $[VOCl_2(tmu)_2]$,[10] suggested that a weak extended exchange interaction of comparable magnitude to the nuclear hyperfine splitting is responsible for the e.s.r. spectra. Four possible modes of extended exchange interaction can be proposed: (*i*) an extended one-dimensional exchange; (*ii*) an extended two-dimensional exchange with two close vanadium–vanadium approaches; [10] (*iii*) an extended two-dimensional exchange with three close vanadium–vanadium approaches; and (*iv*) an extended three-dimensional exchange interaction. Options (*i*) and (*iv*) were quickly discarded as they generally gave simulated spectra with either too few or too many features respectively. Options (*ii*) and (*iii*) were both investigated, but we found that the latter produced the more acceptable simulations. Thus all the simulations shown, see below, are based on option (*iii*) and the segments in Table 1, for which the theoretical treatment is outlined in the Appendix. These simulations assume no changes in the crystal-lattice dimensions with changing temperature. They are also based on only 43.7% of the total possible spectral intensity. For reasons outlined previously,[10] it is computationally too expensive to include the remaining 56.3% of the intensity which is spread over a large number of segments each of which has an extremely small probability. The strategy adopted for simulating the spectra was to obtain, as far as possible, the correct overall width of each spectrum followed by the correct position and relative intensities of as many of the other features as possible. Adequate simulations of the details of the individual spectra for $[H_2tmen][VO(mal)_2(H_2O)]\cdot 2H_2O$ were much more difficult than for $[VOCl_2(tmu)_2]$. The

Table 1. Values of the hyperfine and exchange parameters used in spectrum simulations. Values of $D_{zz}^{T}(\theta)$, $J_{eff.}(\theta)$ and $|K(\theta)|$ are in G; $g_{\parallel} = 1.939$ and $g_{\perp} = 1.974$ when $A_{\parallel} = -183.0$ G and $A_{\perp} = -65.0$ G and when $A_{\parallel} = -190.0$ G, $A_{\perp} = -70.0$ G

		213 K [a]		180 K [b]		155 K [c]		139 K [d]	
θ/°	$D_{zz}^{T}(\theta)$	$J_{eff.}(\theta)$	$\|K(\theta)\|$	$J_{eff.}(\theta)$	$\|K(\theta)\|$	$J_{eff.}(\theta)$	$\|K(\theta)\|$	$J_{eff.}(\theta)$	$\|K(\theta)\|$
0	−20.15	−62.15	183.0	19.87	190.0	69.85	183.0	81.85	190.0
10	−17.72	−59.72	180.5	22.30	187.4	72.28	180.5	84.28	187.4
20	−10.69	−52.70	173.0	29.32	179.8	79.31	173.0	91.31	179.8
30	0.12	−41.88	161.0	40.12	167.6	90.12	161.0	102.12	167.6
40	13.46	−28.54	145.2	53.46	151.5	103.46	145.2	115.46	151.5
50	27.77	−14.23	126.5	67.77	132.4	117.77	126.5	129.77	132.4
60	41.31	−0.69	106.3	81.31	111.8	131.31	106.3	143.31	111.8
70	52.40	10.41	86.7	92.40	91.9	142.41	86.7	154.40	91.9
80	59.70	17.70	71.2	99.70	76.2	149.70	71.2	161.70	76.2
90	62.23	20.23	65.0	102.23	70.0	152.23	65.0	164.23	70.0

[a] $J_0 = -42.0$ G. [b] $J_0 = 40.0$ G. [c] $J_0 = 90.0$ G. [d] $J_0 = 102.0$ G.

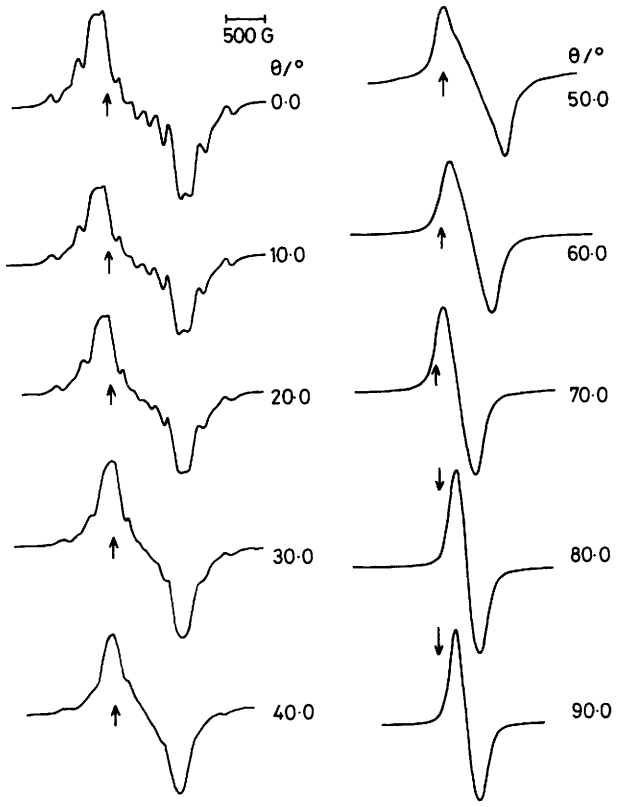

Figure 2. Angular variation of the e.s.r. spectrum in the *bc* plane at 298 K, ν = 9.254 GHz. In Figures 2—6 the applied magnetic field increases from left to right and the arrow indicates an applied magnetic field of 3000 G

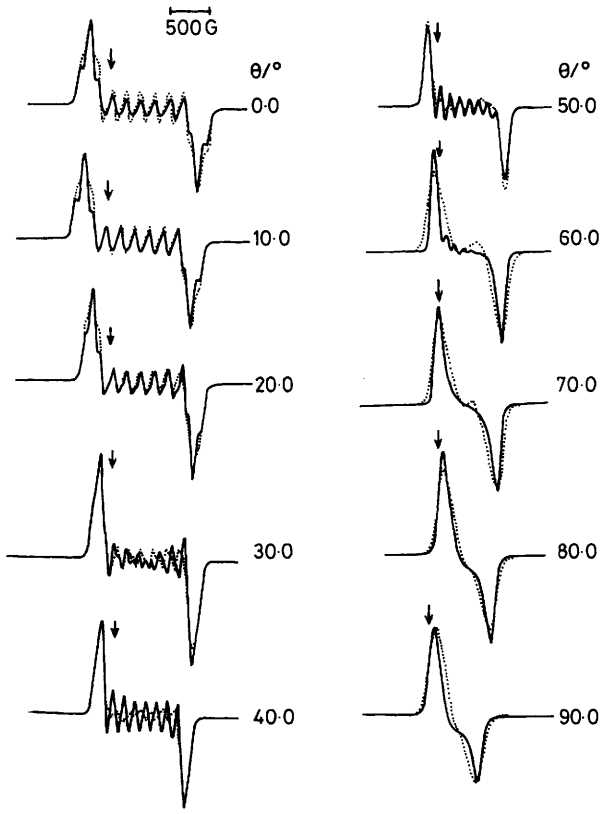

Figure 3. Angular variation of the e.s.r. spectrum in the *bc* plane at 213 K, ν = 9.254 GHz. ——, Experimental; · · · ·, simulated

simulated spectra were more sensitive to variations in linewidth, and indeed it was essential to include an extra linewidth, ΔB_{ω}, for each type of perturbed transition in order to obtain satisfactory simulations. [$\omega J_{eff.}(\theta)$ is the separation between an unperturbed and an exchanged perturbed hyperfine transition, see Appendix and ref. 10.] A similar extra linewidth parameter was also used by Plumlee *et al.*[9] in their interpretation of the e.s.r. spectra of $[NBu^{n}_{4}]_2[Cu(mnt)_2]$. The necessity for this extra linewidth probably arises at least in part from the omission from the simulations of 56.3% of the total available spectral intensity. Values of J_0, $|K(\theta)|$, and $D_{zz}^{T}(\theta)$ used in the simulations are in Table 1, whilst the linewidth parameters $\Delta B_d(\theta)$ and $\Delta B_{\omega}(\theta)$ are in Table 2.

Comparisons of the experimental and simulated spectra at 213, 180, 155, and 139 K are given in Figures 3—6. It should be noted that it is not possible to obtain unique values of $A_{\parallel}$, $A_{\perp}$, and $J_{eff.}(\theta)$ from the simulations, since the effects of these parameters on the simulated spectra are interdependent. We therefore attach no significance to the use of slightly different $A_{\parallel}$ values at the different temperatures. These are merely values which we found gave the best simulations at those temperatures. However, values of $A_{\parallel}$ in the range 180—190 G are not unreasonable since they are compatible with the

Table 2. Linewidth parameters (in G) used in spectrum simulations

θ/°	$\Delta B_d(\theta)$	213 K: $\Delta B_\omega(\theta)$ for $\lvert\omega\rvert$ = 0 ½ 1 3/2 2 5/2 3	180 K: $\Delta B_\omega(\theta)$ for $\lvert\omega\rvert$ = 0 ½ 1 3/2 2 5/2 3	155 K: $\Delta B_\omega(\theta)$ for $\lvert\omega\rvert$ = 0 ½ 1 3/2 2 5/2 3	139 K: $\Delta B_\omega(\theta)$ for $\lvert\omega\rvert$ = 0 ½ 1 3/2 2 5/2 3
0	44.1	100 ← 60 → 10 10	← 30 →	65 ← 45 → 10 10	50 ← 80 → 10 10
10	43.7	100 ← 60 → 10 10	← 30 →	90 ← 65 → 10 10	50 ← 80 → 10 10
20	42.9	100 ← 60 → 10 10	← 30 →	65 ← 90 → 10 10	50 ← 80 → 10 10
30	43.6	100 ← 60 → 10 10	← 25 →	65 ← 90 → 10 10	50 ← 80 → 10 10
40	47.2	100 ← 60 → 10 10	← 10 →	65 ← 90 → 10 10	50 ← 80 → 10 10
50	53.6	100 ← 60 → 10 10	← 30 →	65 ← 90 → 10 10	50 ← 80 → 10 10
60	61.6	← 150 →	← 40 →	65 ← 90 → 10 10	50 ← 80 → 10 10
70	68.9	← 150 →	← 45 →	65 ← 90 → 10 10	50 ← 80 → 10 10
80	74.1	← 150 →	← 60 →	65 ← 90 → 10 10	50 ← 80 → 10 10
90	75.9	← 150 →	← 90 →	65 ← 90 → 10 10	50 ← 80 → 10 10

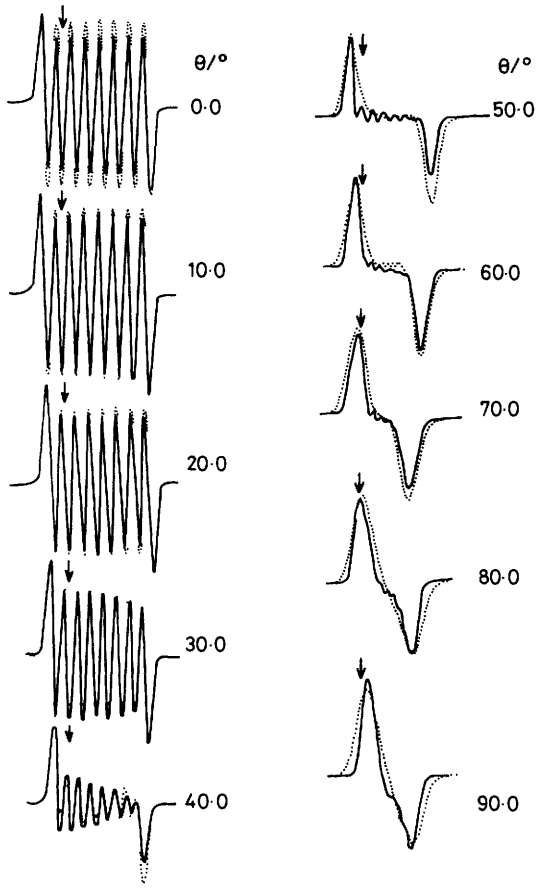

Figure 4. Angular variation of the e.s.r. spectrum in the *bc* plane at 180 K, ν = 9.252 GHz. ——, Experimental; · · · ·, simulated

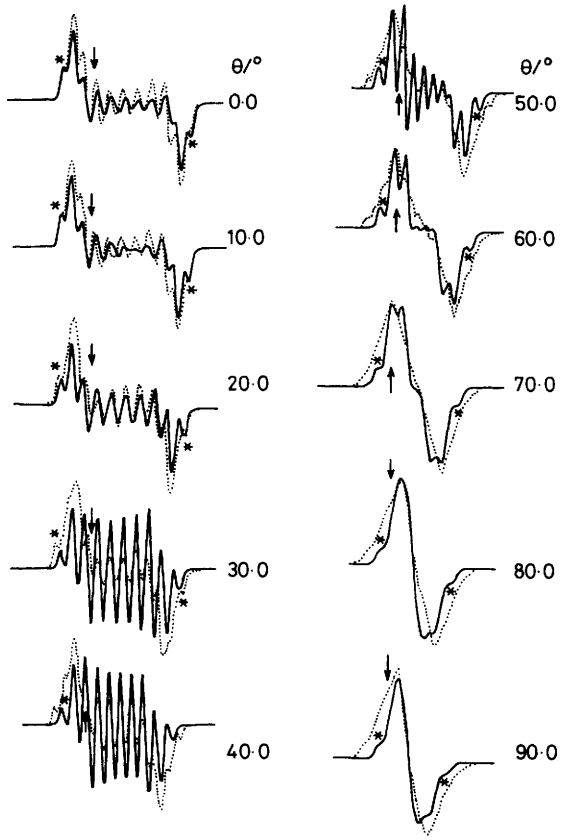

Figure 5. Angular variation of the e.s.r. spectrum in the *bc* plane at 155 K. ν = 9.251 GHz for θ = 0—30° and 9.252 GHz for θ = 40—90°. ——, Experimental; · · · ·, simulated

apparently ' monomeric ' spectra (see below) in the range *ca.* 200—170 K, and are also similar to values found in other oxovanadium(IV) systems.[8,10,14-19] The simulations of the spectra are very good at θ = 0°. However, the simulations for the angular variations of the spectra at 213, 155, and 139 K are only satisfactory over a restricted angular range. Since we are using a perturbation treatment for the definition of our segments, and for calculating the results of the effective exchange, we would expect the model to apply only when $|J_{eff.}(\theta)| < |K(\theta)|$. For comparison only, simulated spectra based on the $|J_{eff.}(\theta)| < |K(\theta)|$ model are shown at angles where this model is strictly not applicable. However, at 155 and 139 K we find that the quality of the simulations deteriorates significantly well before $|J_{eff.}(\theta)| = |K(\theta)|$. Despite this we consider that the simulations support the view that the e.s.r. spectra arise from a weak two-dimensional isotropic exchange interaction. With this as our premise we will now discuss the variation of the e.s.r. spectra with temperature.

For any given $|K(0)|$, $D_{zz}^{T}(0)$, and I, the total width of the spectrum between the weak features (*) Δ(*−*) depends only upon $J_{eff.}(0)$, see equation (A6) in the Appendix. Hence the variation with temperature of the θ = 0 spectra, see Figure 1, particularly with respect to the total width, Δ(*−*), clearly indicates that $|J_{eff.}(0)|$ changes with temperature. The values of $|J_{eff.}(0)|$ decrease with temperature in the range 310—

Table 3. Values of J_0 at different temperatures calculated from $\Delta(*-*)$, equation (A6), and $|K(0)| = 190$ G

T/K	$\Delta(*-*)$/G	$\lvert J_{eff.}(0)\rvert$/G	J_0/G †	T/K	$\Delta(*-*)$/G	$\lvert J_{eff.}(0)\rvert$/G	J_0/G †
4.2	2 440	276	296	190.0	1 425	18	2 or 38
30.0	2 440	276	296	200.0	1 500	32	−12
37.0	2 363	247	267	210.0	1 570	46	−26
52.0	2 288	221	241	220.0	1 688	69	−49
77.0	2 440	205	225	230.0	1 788	91	−71
90.0	2 113	169	189	240.0	1 888	113	−93
105.0	2 025	146	166	250.0	1 975	134	−114
120.0	1 938	125	145	260.0	2 075	159	−139
130.0	1 863	107	127	270.0	2 138	176	−156
140.0	1 750	82	102	280.0	2 213	198	−178
150.0	1 675	67	87	290.0	2 275	217	−197
160.0	1 588	49	69	300.0	2 300	225	−205
170.0	1 513	35	55	310.0	2 400	261	−241
180.0	1 438	20	40				

† Although values of $|J_{eff.}(0)|$ and J_0 are given for the temperature ranges 310—280 and 77—4.2 K, the theory is not strictly applicable over these ranges, since J_0 and $|J_{eff.}(0)|$ are greater than $|K(0)|$

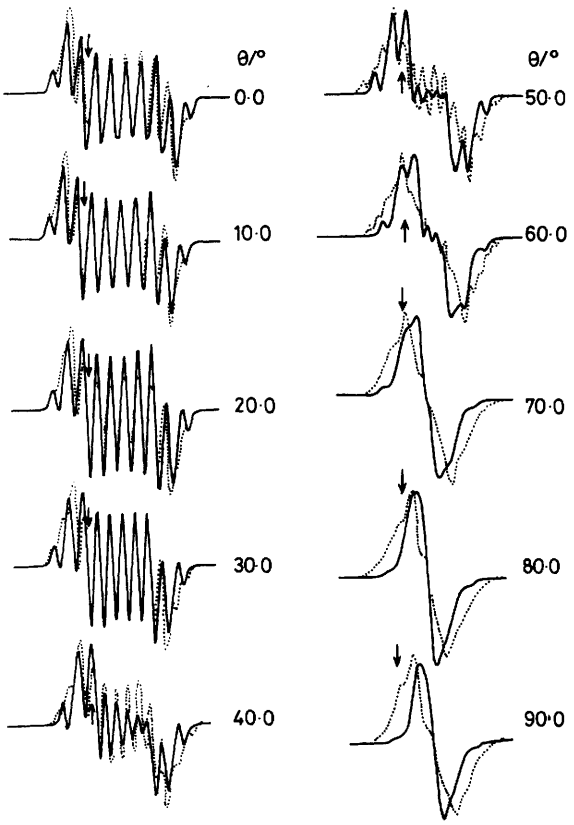

Figure 6. Variation of the e.s.r. spectrum in the *bc* plane at 139 K, $\nu = 9.251$ GHz. ——, Experimental; ····, simulated

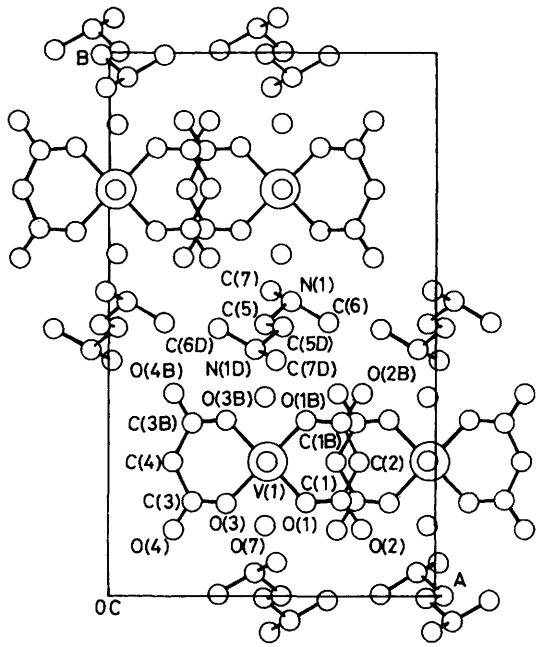

Figure 7. Unit-cell projection of $[H_2tmen][VO(mal)_2(H_2O)]\cdot 2H_2O$ in the *ab* plane

200 K. In the range 200—170 K, $|J_{eff.}(0)|$ goes through either zero or a small minimum value, since the e.s.r. spectra in this range have the appearance of those expected from an isolated monomeric oxovanadium(IV) species.[14] As the temperature is decreased from 170 K, $|J_{eff.}(0)|$ steadily increases with decreasing temperature. Values of $|J_{eff.}(0)|$ calculated using equation (A6) for a fixed value of $A_{\parallel} = 190$ G are given in Table 3. Only the absolute value of $J_{eff.}(\theta)$ affects the simulated e.s.r. spectrum. However, since $J_{eff.}(\theta) = J_0 + D_{zz}^{T}(\theta)$ and $D_{zz}^{T}(\theta)$ is of fixed magnitude and sign for a given θ and crystal structure, any absolute value of $J_{eff.}(\theta)$ may arise from two possible values of J_0 which are *opposite* in sign. Thus the intriguing question arises, does the sign of J_0 change as $|J_{eff.}(0)|$ goes through its minimum value? As indicated below we believe we have strong evidence to show that J_0 does indeed change sign in the temperature range 200—170 K.

The basis for this conclusion is the angular variation of the e.s.r. spectra. Assuming that the structure does not change, each $D_{zz}^{T}(\theta)$ will remain constant with temperature. However, $|J_{eff.}(\theta)|$ will vary with θ in a different way for different values of J_0. Thus if we choose two temperatures where $|J_{eff.}(0)|$ values are equal, the angular variation of the spectra at these two temperatures should distinguish between the two possible signs of J_0 which can produce the same $|J_{eff.}(0)|$. As near as was practicable, two temperatures at which the $\theta = 0$ spectra were identical are 213 and 155 K. The simulations gave $|J_{eff.}(0)| = 62.1$ G at 213 K and 69.85 G at 155 K. Thus the possible values of J_0 are +82.3 or −42.0 G

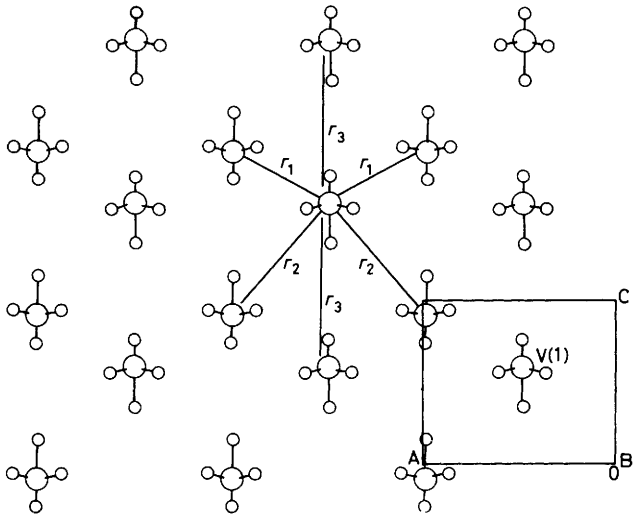

Figure 8. The packing of the $[VO(mal)_2(H_2O)]^{2-}$ anions in the layer parallel to the *ac* plane. Only the vanadium atoms (large circles) and the oxygen atoms (small circles) co-ordinated to vanadium are shown

at 213 K and +90.0 or −49.7 G at 155 K. Because of the value of $D_{zz}^{T}(\theta)$, and the way in which it varies with θ, either of the negative J_0 values leads to $|J_{eff.}(\theta)|$ which is initially small, decreases with increasing θ to zero at *ca.* θ = 60°, and then increases slightly up to θ = 90°, see Table 1. Hence we would predict that as θ is increased from zero the spectrum should tend towards and reach that of a monomeric system, *cf.* the spectra at 180 K (Figure 4) and those of $[VOCl_2(OPPh_3)_2]$.[14] This is indeed what is observed for the spectra obtained at 213 K, and successfully simulated on this basis. Thus a negative value of J_0 (ferromagnetic) is applicable at this and presumably the higher temperatures. On the other hand the positive J_0 values result in $|J_{eff.}(\theta)|$ which steadily increases as θ increases (see Table 1). We would therefore anticipate that the e.s.r. spectra should resemble those for a weakly exchanging system at all values of θ. Although we have been unable accurately to simulate the spectra obtained at 155 K for all values of θ, the presence of the weak features (*) at all angles of θ, and the occurrence, up to θ = 50°, of more than the eight features expected from a monomeric system, qualitatively support the assumption of a positive value of J_0 (antiferromagnetic). The signs associated with the J_0 values in Table 3 were derived on this basis.

The possibility that the above changes in J_0 could be due to changes in $D_{zz}^{T}(0)$ with temperature was considered. If each vanadium–vanadium distance is allowed to vary by ±0.5 Å from the positions determined at room temperature, then the maximum shift in $D_{zz}^{T}(0)$ is −30 G. Thus, allowing relatively large changes in vanadium–vanadium distances with temperature does not lead to the observed change in $|J_{eff.}(0)|$ or to the change in sign of J_0.

The observed variation of J_0 with temperature suggests that there could be both a ferromagnetic and antiferromagnetic contribution to the isotropic exchange, one or both of which varies with temperature. Because of the small magnitude of the electronic exchange interactions it is difficult to be certain of their origins, but the crystal structure does suggest some possibilities. There could be a direct interaction between the $d_{x^2-y^2}$ orbitals on adjacent centres in the layer. [We assume that the *x* and *y* axes on each individual vanadium centre are between the malonato–oxygen atoms thus giving a $(d_{x^2-y^2})^1$ ground state.] The relatively large distances involved would be expected to result in only a weak interaction. However, it is not obvious that such a mechanism would lead to the observed change in J_0 as the temperature changes. A change in the exchange interaction from ferromagnetic in the solid to antiferromagnetic in frozen solutions has been reported for each of the compounds bis(*N*-methylsalicylideneiminato)-copper(II) [20] and bis(dimethylglyoximato)copper(II).[20,21] These changes in the sign of the exchange interaction were attributed, at least in part, to an increase in the copper–copper separation on changing from the solid to solution phase.[20–22] However, we would expect the vanadium–vanadium separations to decrease with decreasing temperature and thus our observed change in sign of J_0 is opposite to that observed for these copper compounds. This suggests that a direct interaction between metal orbitals is not responsible for the exchange in our system.

A superexchange mechanism is possible *via* the malonato-ligands. Figure 7 shows that there is possible overlap, particularly of the carbonyl groups, of the malonato-ligands on adjacent anions. Again the distances, number of atoms, and types of orbitals involved indicate a weak antiferromagnetic contribution.[23–26] Mechanisms for the ferromagnetic contribution are more difficult to envisage. If the symmetry of a single vanadium centre is less than axial, for example C_{2v}, there could be mixing of the metal $d_{x^2-y^2}$ and d_{z^2} orbitals. Interaction between the d_{z^2} orbitals on adjacent vanadiums, *via* a $^{-}V{=}O\cdots H_2O{-}V{=}O\cdots$ system parallel to the *c* axis, would effectively allow the transfer of an electron between different types of orbitals on the adjacent centres, thus leading to a ferromagnetic exchange contribution.[25,26] Since the extent of metal *d*-orbital mixing is likely to be small, the vanadium–vanadium distance is large (r_3 = 9.434 Å), and there are a large number of intervening atoms, we would expect such an interaction to be small in magnitude.

An almost linear variation of the nearest-neighbours exchange, *J*, from *J ca.* 0.05 K at 300 K to *J ca.* 0.027 K at 77 K has been reported for $K_2CuCl_4{\cdot}2H_2O$.[27] The pathway for exchange was assumed to be *via* $Cu{-}Cl\cdots H_2O{-}Cu{-}$, whilst the temperature variation of the exchange was attributed to the thermal occupation of an optical mode. This would seem unlikely in the present vanadium system since the lowest optical transition in this, and in other oxovanadium(IV) systems,[28] occurs at energies greater than 10^4 cm^{-1}. A possible explanation advanced by Plumlee *et al.*[9] to explain the approximate three-fold increase in J_0 between 4.2 and 300 K for $[NBu^n_4]_2[Cu(mnt)_2]$ was that of superexchange involving various molecular orbitals between adjacent sites. The increase in J_0 was rationalised in terms of improved effective overlap with increasing vibrational amplitude. A similar mechanism could be invoked in $[H_2tmen][VO(mal)_2(H_2O)]{\cdot}2H_2O$, whereby ligand vibrations could effect overlap between molecular orbitals involving metal $d_{x^2-y^2}$ on one centre and say metal d_{xy} on the adjacent centre. Because the effective transfer of electrons between the two sites would involve different types of orbitals on the two centres, it should result in a ferromagnetic contribution.[25,26] Any of the above exchange mechanisms, which involve ligand–ligand interactions, are likely to be sensitive to ligand vibrations. Thus their contributions to the exchange interaction could well be temperature dependent.

Appendix

The theoretical approach to the interpretation of the e.s.r. spectra is that given in the preceding paper,[10] modified to include the possibility of three close approaches. In order to simplify the exchange operators and reduce the computation time we have again assumed that the component dipolar

Table A1. Statistical weighting for various segments in a two-dimensional layer of vanadium centres for three close approaches

Length of segment	Statistical weighting
(*a*) $N = 1, m = 6$	
$L_1 = L_2 = L_3 = L_4 = L_5 = L_6 = 1$	0.2014
$L_1 = L_2 = L_3 = L_4 = L_5 = 1, L_6 = 2$ + 5 other possible combinations	0.1511
$L_1 = L_2 = L_3 = L_4 = 1, L_5 = L_6 = 2$ + 14 other possible combinations	0.0472
$L_1 = L_2 = L_3 = 1, L_4 = L_5 = L_6 = 2$ + 19 other possible combinations	0.0079
(*b*) $N = 2, m = 8$	
$L_1 = L_2 = L_3 = L_4 = L_5 = L_6 = L_7 = L_8 = 1$	0.0295

interactions $D_{zz}^{(1)}(\theta)$, $D_{zz}^{(2)}(\theta)$, and $D_{zz}^{(3)}(\theta)$ may be summed to give a nett dipolar contribution $D_{zz}^{T}(\theta)$. With these assumptions the nett exchange operators for a central monomer ($N = 1$) become as in equations (A1) and (A2). The first- and second-order corrections to resonance fields are then as in equation (A3), where $J_{eff.}(\theta) = J_0 + D_{zz}^{T}(\theta)$, and (A4) where $C^T = [J_0 - \frac{1}{2}D_{zz}(\theta)]/4K(\theta)$.

$$V_N(\|) = J_{eff.}(\theta)(\hat{S}_1^z\hat{S}_N^z + \hat{S}_2^z\hat{S}_N^z + \hat{S}_3^z\hat{S}_N^z + \hat{S}_N^z\hat{S}_4^z + \hat{S}_N^z\hat{S}_5^z + \hat{S}_N^z\hat{S}_6^z) \quad \text{(A1)}$$

$$V_N(\perp) = \tfrac{1}{2}[J_0 - \tfrac{1}{2}D_{zz}^{T}(\theta)](\hat{S}_1^+\hat{S}_N^- + \hat{S}_1^-\hat{S}_N^+ + \hat{S}_2^+\hat{S}_N^- + \hat{S}_2^-\hat{S}_N^+ + \hat{S}_3^+\hat{S}_N^- + \hat{S}_3^-\hat{S}_N^+ + \hat{S}_N^+\hat{S}_4^- + \hat{S}_N^-\hat{S}_4^+ + \hat{S}_N^+\hat{S}_5^- + \hat{S}_N^-\hat{S}_5^+ + \hat{S}_N^+\hat{S}_6^- + \hat{S}_N^-\hat{S}_6^+) \quad \text{(A2)}$$

$$H^{(1)}(\theta) = \frac{1}{N}\cdot J_{eff.}(\theta)(F_{L_1} + F_{L_2} + F_{L_3} + F_{L_4} + F_{L_5} + F_{L_6}) = \omega J_{eff.}(\theta) \quad \text{(A3)}$$

$$H^{(2)}(\theta) = \frac{C^T}{N}\left(\frac{1}{M_I^N - M_I^{L_1}} + \frac{1}{M_I^N - M_I^{L_2}} + \frac{1}{M_I^N - M_I^{L_3}} + \frac{1}{M_I^N - M_I^{L_4}} + \frac{1}{M_I^N - M_I^{L_5}} + \frac{1}{M_I^N - M_I^{L_6}}\right) \quad \text{(A4)}$$

$$\left.\begin{aligned} \text{For } M_I^N = \pm\tfrac{7}{2},\ H^{(2)}(\theta) &= \frac{C^T}{N}(\pm 2.2224) \\ M_I^N = \pm\tfrac{5}{2},\ H^{(2)}(\theta) &= \frac{C^T}{N}(\pm 1.2429) \\ M_I^N = \pm\tfrac{3}{2},\ H^{(2)}(\theta) &= \frac{C^T}{N}(\pm 0.6714) \\ M_I^N = \pm\tfrac{1}{2},\ H^{(2)}(\theta) &= \frac{C^T}{N}(\pm 0.2143) \end{aligned}\right\} \quad \text{(A5)}$$

Similar equations to (A1)—(A5) may be derived for a central dimer.

The segments used in the simulations which individually gave a significant statistical contribution to the total spectrum are given in Table A1. These segments gave rise to 9 728 transitions and accounted for 43.7% of the total spectral intensity. The simulations were achieved as described in ref. 10, equations (A33)—(A37). The total linewidth, ΔB, used in the simulations was composed from two parts. (*i*) A Van Vleck dipolar linewidth $\Delta B_d(\theta)$ computed according to equation (A37) in ref. 10. The inter-vanadium separations which were explicitly included in the exchange operator were not included in this linewidth calculation. (*ii*) An additional linewidth parameter, $\Delta B_\omega(\theta)$, was introduced so that transitions with different ω values (*i.e.* $|\omega| = 0, \frac{1}{2}, 1, \frac{3}{2}, 2, \frac{5}{2}$, and 3) could be attributed different linewidths. This is similar to the device used by Plumlee *et al.*,[9] and by us for $[VOCl_2(tmu)_2]$.[10] The assignment of different linewidths to different perturbed transitions was essential for a reasonable simulation of the details within a spectrum.

Expression (A6) for the total width of the spectrum, $\Delta(*{-}*)$, between the weak features (*) which arise from the maximum exchange splitting ($|\omega| = 3$) may be derived from equations (A3)—(A5). The first term in this equation is the

$$\Delta(*{-}*) = 2I|K(\theta)| + 6(J_{eff.}\theta) - \frac{4.444[J_{eff.}(\theta) - \frac{3}{2}D_{zz}^{T}(\theta)]^2}{4|K(\theta)|} \quad \text{(A6)}$$

contribution from the hyperfine splitting, the second is the first-order exchange, whilst the third represents the second-order exchange contribution. Thus, from calculated values of $K(\theta)$ and $D_{zz}^{T}(\theta)$, and the measured $\Delta(*{-}*)$, values of $\left|\frac{J_{eff.}(\theta)}{J_{eff.}(\theta)}\right|$ can be obtained. There are in fact two values of $\left|\frac{J_{eff.}(\theta)}{J_{eff.}(\theta)}\right|$, but one represents a situation where the second-order term dominates the first-order term and can be rejected.

Acknowledgements

We thank the S.E.R.C. for financial support. Computations were performed on the University of Manchester Regional Computer Centre ICL 1900/CDC 7600 Joint System. Diagrams of the crystal structures were obtained using PLUTO78 from the Cambridge Crystallographic Files.

References

1 A. Abragam and B. Bleaney, ' Electron Paramagnetic Resonance of Transition Ions,' Clarendon Press, Oxford, 1970.
2 B. Bleaney and K. D. Bowers, *Philos. Mag.*, 1952, **43**, 372; *Proc. R. Soc. London, Ser. A*, 1952, **214**, 451.
3 H. Abe and J. Shimada, *Phys. Rev.*, 1953, **90**, 316; *J. Phys. Soc. Jpn.*, 1957, **12**, 1255.
4 C. J. Gorter and J. H. Van Vleck, *Phys. Rev.*, 1947, **72**, 1128.
5 J. H. Van Vleck, *Phys. Rev.*, 1948, **74**, 1168.
6 P. W. Anderson and P. R. Weiss, *Rev. Mod. Phys.*, 1953, **25**, 269.
7 Z. G. Soos, R. T. McGregor, T. T. P. Cheung, and A. J. Silverstein, *Phys. Rev. B*, 1977, **16**, 3036.
8 G. D. Simpson, R. L. Belford, and R. Biagioni, *Inorg. Chem.*, 1978, **17**, 2424.
9 K. W. Plumlee, B. M. Hoffmann, J. A. Ibers, and Z. G. Soos, *J. Chem. Phys.*, 1975, **63**, 1926.
10 B. Gahan and F. E. Mabbs, preceding paper.
11 D. Snaathorst, H. M. Doesburg, J. A. A. J. Perenboom, and C. P. Keijzers, *Inorg. Chem.*, 1981, **20**, 2526.
12 A. Pajunen and S. Pajunen, *Acta Crystallogr., Sect. B*, 1980, **36**, 2425.
13 C. D. Garner, P. Lambert, F. E. Mabbs, and J. K. Porter, *J. Chem. Soc., Dalton Trans.*, 1972, 320.
14 B. Gahan and F. E. Mabbs, following paper.
15 H. A. Kuska and P-H. Yang, *Inorg. Chem.*, 1974, **13**, 1090.
16 J. M. Flowers, J. C. Hempel, W. E. Hatfield, and H. H. Dearman, *J. Chem. Phys.*, 1973, **58**, 1479.
17 K. K. Sunil and M. T. Rogers, *Inorg. Chem.*, 1981, **20**, 3283.
18 A. Jezierski and B. J. Raynor, *J. Chem. Soc., Dalton Trans.*, 1981, 1.
19 K. P. Callahan and P. J. Durand, *Inorg. Chem.*, 1980, **19**, 3211.
20 M. Chikira and T. Isobe, *Chem. Phys. Lett.*, 1975, **30**, 498.

21 T. D. Smith and J. R. Pilbrow, *Coord. Chem. Rev.*, 1974, **13**, 173.
22 M. Chikira and T. Isobe, *Bull. Chem. Soc. Jpn.*, 1972, **45**, 3006.
23 J. B. Goodenough, *Phys. Chem. Solids*, 1958, **6**, 287.
24 J. Kanamori, *Phys. Chem. Solids*, 1959, **10**, 87.
25 P. W. Anderson, *Solid State Phys.*, 1963, **14**, 99.
26 J. Owen and J. H. M. Thornley, *Rep. Prog. Phys.*, 1966, **29**, 675.
27 T. A. Kennedy, S. H. Choh, and G. Seidel, *Phys. Rev. B*, 1970, **2**, 3645.
28 D. Collison, B. Gahan, C. D. Garner, and F. E. Mabbs, *J. Chem. Soc., Dalton Trans.*, 1980, 667.

Received 4th October 1982; *Paper* 2/1709